Human Cancer Biology

Clinical Cancer Research

Impact of Tumor Microenvironment and Epithelial Phenotypes on Metabolism in Breast Cancer

Heather Ann Brauer[1], Liza Makowski[2,3], Katherine A. Hoadley[3], Patricia Casbas-Hernandez[4], Lindsay J. Lang[1], Erick Romàn-Pèrez[1], Monica D'Arcy[1], Alex J. Freemerman[2], Charles M. Perou[3,4,5], and Melissa A. Troester[1,3,4]

Abstract

Purpose: Cancer cells have altered metabolism, with increased glucose uptake, glycolysis, and biomass production. This study conducted genomic and metabolomic analyses to elucidate how tumor and stromal genomic characteristics influence tumor metabolism.

Experimental Design: Thirty-three breast tumors and six normal breast tissues were analyzed by gene expression microarray and by mass spectrometry for metabolites. Gene expression data and clinical characteristics were evaluated in association with metabolic phenotype. To evaluate the role of stromal interactions in altered metabolism, cocultures were conducted using breast cancer cells and primary cancer-associated fibroblasts (CAF).

Results: Across all metabolites, unsupervised clustering resulted in two main sample clusters. Normal breast tissue and a subset of tumors with less aggressive clinical characteristics had lower levels of nucleic and amino acids and glycolysis byproducts, whereas more aggressive tumors had higher levels of these Warburg-associated metabolites. While tumor-intrinsic subtype did not predict metabolic phenotype, metabolic cluster was significantly associated with expression of a wound response signature. In cocultures, CAFs from basal-like breast cancers increased glucose uptake and basal-like epithelial cells increased glucose oxidation and glycogen synthesis, suggesting interplay of stromal and epithelial phenotypes on metabolism. Cytokine arrays identified hepatocyte growth factor (HGF) as a potential mediator of stromal–epithelial interaction and antibody neutralization of HGF resulted in reduced expression of glucose transporter 1 (*GLUT1*) and decreased glucose uptake by epithelium.

Conclusions: Both tumor/epithelial and stromal characteristics play important roles in metabolism. Warburg-like metabolism is influenced by changes in stromal–epithelial interactions, including altered expression of HGF/Met pathway and *GLUT1* expression. *Clin Cancer Res; 19(3); 571–85. ©2012 AACR.*

Introduction

Highly proliferative tumor cells undergo fundamental changes in metabolism and nutrient usage to survive and progress (1), and metabolic transformation appears to be necessary for sustained proliferation (2). Much of the metabolic transformation is glucose-dependent, with invasive cancers exhibiting increased aerobic glycolysis (3) via the "Warburg Effect" (4). The Warburg effect occurs when there is a metabolic shift toward glycolysis, with increased cellular production of biomass, especially amino acids and nucleic acids. While the Warburg phenomenon has been investigated for more than 85 years, the metabolic interactions between stroma and epithelium are not well characterized, despite the important role of stroma in breast cancer biology (5–12).

The gap in our understanding of stromal–epithelial interactions was recently illuminated when it was shown that epithelial tumor cells induce oxidative stress in the normal stroma (9), in turn, leading to activation of NFκB and hypoxia-inducible-1α (HIF-1α) pathways in cancer-associated fibroblasts (CAF; ref. 11). Concomitant changes in inflammation, autophagy, mitophagy, and aerobic glycolysis are induced in the stroma, which then produces energy-rich metabolites (such as lactate and pyruvate) that are secreted and used by epithelial cells to generate ATP (11, 13). This bidirectional communication, with aerobic glycolysis in stroma fueling cancer growth is referred to as "Reverse Warburg Effect" (14–16), and its discovery established an important role for stroma in altering metabolism (9–11). However, differences in metabolomics by stromal–epithelial interaction and according to breast cancer subtype have not been widely investigated.

Authors' Affiliations: Departments of [1]Epidemiology and [2]Nutrition, Gillings School of Global Public Health; [3]Lineberger Comprehensive Cancer Center; Departments of [4]Pathology and Laboratory Medicine and [5]Genetics, School of Medicine, University of North Carolina at Chapel Hill, Chapel Hill, North Carolina

Note: Supplementary data for this article are available at Clinical Cancer Research Online (http://clincancerres.aacrjournals.org/).

Corresponding Author: Melissa A. Troester, University of North Carolina at Chapel Hill, 135 Dauer Drive, Chapel Hill, NC 27599. Phone: 919-966-7408; Fax: 919-966-2089; E-mail: troester@unc.edu

doi: 10.1158/1078-0432.CCR-12-2123

©2012 American Association for Cancer Research.

Downloaded from http://aacrjournals.org/clincancerres/article-pdf/19/3/571/2296963/571.pdf by guest on 24 August 2022

Translational Relevance

Evolutionary theories of cancer argue that tumors must adapt to their local microenvironments to progress, including adaptation to limited oxygen and nutrients. While evolution of breast cancers appears to result in distinct genomic subtypes, the corresponding metabolomic subtypes have not been well characterized. We provide evidence that metabolomic characteristics of tumors are a result of complex interactions between stromal and cancer cells, with stromal–epithelial interactions playing a critical role in substrate metabolism observed in tumors. More aggressive cancers possess a distinct metabolic phenotype, which is weakly associated with cancer subtype, and more strongly associated with expression of a stroma-derived wound response signature. Several studies have suggested that metabolic phenotypes of tumors may be targetable to inhibit tumor growth, but an understanding of the genomic controls upon tissue metabolism is needed. We show that glucose uptake in epithelial cells, occurs partially through glucose transporter 1 (GLUT1) receptor. Epithelial *GLUT1* expression, in turn, is dependent upon coculture-derived hepatocyte growth factor (HGF) secretion. Because HGF/c-MET pathway is implicated in other malignancies and c-MET inhibitors are already clinically available, blocking c-MET response to HGF may be a plausible strategy for targeting tumor metabolism.

Breast tumors show substantial heterogeneity (17) with at least 5 distinct subtypes: luminal A, luminal B, HER2-positive, basal-like, and claudin-low breast cancers (18–20). In addition to their unique cell-autonomous characteristics [including unique mutation patterns, chemotherapy responses, and cellular phenotypes (21–23)], these subtypes have distinct interactions with the stroma. The interaction of basal-like breast cancer cells with fibroblasts leads to an increase in inflammatory cytokines and migratory behavior, whereas luminal cells in culture with fibroblasts show distinct gene expression and altered proliferation (12, 24). This evidence of subtype-specific interactions with surrounding stroma underscores the importance of studying epithelial and stromal factors simultaneously when evaluating tumor metabolism.

In the present study, we apply metabolomics and radiotracer metabolic studies to simultaneously investigate the role of tumor gene expression and stromal–epithelial interactions in tumor metabolism. Tissue samples were used to conduct gene expression analyses and samples were classified using multiple published signatures: the PAM50 signature, claudin-low signature, and *in vivo* wound response signature (17, 20, 25). These gene expression phenotypes were then compared with metabolomics classes identified by analysis of 379 metabolites. Complementary coculture experiments were carried out to evaluate subtype-specific metabolic interactions of stromal and epithelial cells experimentally. Our results illustrate that compared with luminal cancer cells or luminal-derived CAFs, basal-like cells and basal-like CAFs play a strong role in determining substrate metabolism in culture. Strong associations between tissue metabolic phenotype and tissue gene expression also suggest the importance of stroma in metabolic cancer microenvironments.

Materials and Methods

Patient samples

Thirty-one fresh-frozen breast tumor samples, 6 breast tissue samples from reduction mammoplasty, and 5 metastatic samples were obtained under Institutional Review Board (IRB)-approved protocols at the University of North Carolina at Chapel Hill (UNC-CH; Chapel Hill, NC). Patients were treated according to the standard of care dictated by disease stage, estrogen response (ER), and HER2 status. Table 1 describes patient demographics and tumor characteristics. All tissues were handled by snap freezing immediately after surgery, and RNA was isolated using a protocol as described by Hu and colleagues (26). RNA integrity was determined using the RNA 6000 Nano LabChip Kit and Agilent 2100 Bioanalyzer.

Microarrays

Microarrays experiments were carried out as described (26). Briefly, labeled cRNA was generated using Agilent's Low RNA Input Linear Amplification Kit. Cy5-labeled experiment samples were combined with Cy3-labeled reference (Stratagene Universal Human Reference spiked with 1:1,000 with MCF-7 RNA and 1:1,000 with ME16C RNA to increase expression of breast cancer genes) and hybridized to 4 × 44 K Agilent whole genome arrays or 244 K Agilent custom arrays. For 2 cases with duplicate arrays, the intraclass correlation coefficients (ICC) were 0.597 and 0.886, suggesting moderate-to-strong agreement between replicates. All tumor gene expression data are publicly available through the Gene Expression Omnibus (GSE6128 and GSE6130).

Metabolite arrays

For each tumor, a single sample was analyzed for metabolites. Tissue (100 mg) was homogenized in a volume of water at 4 μL per mg of sample in a 2-mL cryovial with two 3-mm zirconium oxide beads, one 3:8 steel ballcone, and one 1:8 steel ballcone on the GenoGrinder at 1,000 strokes/min for 5 minutes. A 100 μL aliquot of the homogenate was placed in a 96-well deepwell plate along with two 3-mm zirconium oxide grinding beads per well. The plate was placed in the chiller on the robot, and a 400 μL volume of EtOAc/EtOH (1:1) with 2.5 μg/mL 2-fluorophenylglycine and 25 μg/mL d2-maleic acid and tridecanoic acid was added to each well. The plate was capped with a plate mat and samples were shaken on GenoGrinder at 675 strokes/min for 2 minutes. The plate was centrifuged on a Beckman GS-6R centrifuge at 3,200 rpm for 5 minutes at 4°C and then placed back on the Hamilton LabStar robot and the centrifugates were transferred to a second plate. A 200-μL

Downloaded from http://aacrjournals.org/clincancerres/article-pdf/19/3/571/2296963/571.pdf by guest on 24 August 2022

Table 1. Characteristics of breast cancer samples by two clusters according to metabolite expression

	Total	Cluster 1—good prognosis ($N = 18$)	Cluster 2—poor prognosis ($N = 15$)	
	N	*n* (%)	*n* (%)	*P*
ER status				
Positive	20	13 (61.1)	7 (38.9)	
Negative	10	3 (41.7)	7 (58.3)	0.122
Missing	3	2 (66.7)	1 (33.3)	
Size				
≤2 cm	7	7 (100)	0 (0)	
>2–≤5 cm	12	5 (41.7)	7 (58.3)	
>5 cm	5	2 (40)	3 (60)	0.047
Direct extension to chest wall or skin	7	3 (42.9)	4 (57.1)	
Missing	2	1 (50)	1 (50)	
Tumor subtype[a]				
Basal	10	4 (40)	6 (60)	
HER2	3	1 (66.7)	2 (33.3)	
Luminal A	10	9 (90)	1 (10)	0.064
Luminal B	6	2 (33.3)	4 (66.7)	
Claudin-low	3	1 (33.3)	2 (66.7)	
Normal-like	1	1 (100)	0 (0)	
Tumor grade				
Well-differentiated/1	2	2 (100)	0 (0)	
Intermediate/2	7	5 (71.4)	2 (28.6)	0.135
Poorly differentiated/3	20	8 (40)	12 (60)	
Missing	4	3 (75)	1 (25)	
Node[b]				
Negative	21	12 (57.1)	9 (42.9)	
Positive	10	5 (50)	5 (50)	0.991
Unknown	2	1 (50)	1 (50)	
Age, y				
30–39	5	2 (40)	3 (60)	
40–49	5	3 (60)	2 (40)	
50–59	5	3 (60)	2 (40)	0.952
≥60	16	9 (56.3)	7 (43.7)	
Unknown	2	1 (50)	1 (50)	

[a]Classified using PAM50 algorithm applied to microarray data.
[b]Negative means no positive lymph nodes. Positive is at least one positive lymph node.

volume of MeOH was placed in each well of the first plate, and the plate was shaken and centrifuged as before. The centrifugates were transferred as before and the same process was repeated using 200 μL volume of MeOH/H2O (3:1) and then repeated using 200 μL volume of DCM/MeOH (1:1). The samples were mixed by pipetting up and down several times and a 225 μL aliquot of each was transferred to each of two 250-μL autosampler vial inserts. All extracts were placed in the Zymark TurboVap 96 for concentration under nitrogen streams for 25 minutes. A second 225 μL aliquot of each sample was transferred to the appropriate insert, and the samples were placed in the Labconco Centrivap Concentrator for drying for 6.5 hours for drying. Samples were transferred to the Labconco Freezone 6 lyophilizer for further overnight drying. For liquid chromatography/mass spectrometry (LC/MS), a 40-μL volume of MeOH with 20 μg/mL D10 benzophenone was added to each sample. Samples were shaken with a Lab-Line Titer plate shaker for 5 minutes on setting 7 and then a 60 μL volume of 0.1% formic acid was added containing 5 μg/mL d3 leucine, 5 μg/mL DL-4-chlorophenylalanine, 5 μg/mL 4-bromo-DL-phenylalanine, and 0.5 μg/mL amitryptyline.

For gas chromatography/mass spectrometry (GC/MS), samples were derivatized to a final volume of 50 μL for GC/MS analysis using equal parts bistrimethyl-silyl-trifluoroacetamide and solvent mixture acetonitrile:dichloromethane:cyclohexane (5:4:1) with 5% triethylamine at 60°C for 1 hour. Three types of controls were analyzed in concert with the experimental samples: samples generated from pooled experimental samples served as technical

Downloaded from http://aacrjournals.org/clincancerres/article-pdf/19/3/571/2296963/571.pdf by guest on 24 August 2022

replicates throughout the data set, extracted water samples served as process blanks, and a cocktail of standards spiked into every analyzed sample allowed instrument performance monitoring. Experimental samples and controls were randomized across the platform run. Raw data are included in Supplementary Table S1.

Metabolite data analysis

Metabolite levels with signal intensity greater than 10 dpi in both channels and at least 80% present data were selected and the red/green Lowess-normalized ratios for each gene were $\log_2$-transformed. Missing data were imputed using k-nearest neighbors' imputation (with $k = 10$). This resulted in a complete dataset consisting of 379 metabolites, and each row/metabolite was median-centered. Data were analyzed by unsupervised significance analysis of microarray (SAM; ref. 27), and significant metabolites were clustered across all samples using average-linkage hierarchical cluster analysis, results were visualized using Java Treeview (28). SAM uses the variance structure of the data to compute expected distributions. Small fold changes were statistically significant by SAM analysis due to low variation between samples within a class. To test whether there was a significant trend in metabolite level for classes of metabolites [amino acids, carbohydrates/sugars, nucleic acids, and the tricarboxylic acid (TCA) cycle metabolites], we estimated the β-value and P value corresponding to linear regression of metabolite level on an ordinal variable equal to 1 for normal tissue, 2 for cluster 1 samples, 3 for cluster 2 samples, and 4 for metastases. Statistical tests of the trend were 2-tailed and SE was calculated (SAS version 9.2). Because these clusters emerged from SAM analyses where multiple comparisons were adjusted, no adjustment for multiple comparisons was made in the trend analyses. The objective of these analyses is to show whether there is evidence of a monotonic increase or decrease in metabolite level.

Gene expression data analysis

Using the probe set common to both array platforms (25), probes with signal intensity greater than 10 dpi in both channels and at least 80% present data were selected and the red/green Lowess-normalized ratios for each gene were $\log_2$-transformed. Duplicate microarrays corresponding to the same patient sample were combined by averaging. Missing data were imputed using k-nearest neighbors' imputation (with $k = 10$). Gene annotations from each dataset were mapped to UniGene cluster IDs (UCIDs, Build 161) using the SOURCE database, and multiple occurrences of a UCID were collapsed by taking the median value for that ID within each experiment and platform. This resulted in a complete dataset consisting of about 2,800 genes, and each experiment was standardized to N(0, 1) and each row/gene was median-centered.

To identify genes that significantly changed by metabolic cluster (cluster 1 or 2), data were analyzed by 2-class SAM (27). Significant genes were clustered across all samples using average-linkage hierarchical cluster analysis, and results were visualized using Java Treeview (28). Significant genes were evaluated for ontologic enrichment using Ingenuity Pathway Analysis (IPA), with Benjamini–Hochberg (B–H) multiple testing correction. Significant functions and pathways were defined as those with B–H $P < 0.05$.

Associations between metabolic phenotype and biologically defined gene expression signatures

To characterize the biologic phenotypes of the metabolic clusters, gene expression in each sample was compared with an existing *in vivo* breast-derived wound response signature (25). The wound response signature was generated by comparing cancer-adjacent stroma-rich breast tissue to breast tissue from reduction mammoplasty, which identified an active wound signature in the cancer-adjacent tissue. The median-centered gene expression profile of each patient was evaluated for correlation with this signature by calculating Pearson correlation coefficients, using the method of Creighton and colleagues (29). Briefly, vectors corresponding to the genes in the wound response signature were constructed, with 1 assigned to upregulated genes and −1 assigned to downregulated genes. Sample arrays were filtered to retain only genes with interquartile range (IQR) of at least 0.8. A Pearson correlation coefficient was calculated comparing this standard vector to the vector of median-centered gene expression for each patient. Patients were classified as positive if the Pearson correlation coefficient was greater than zero and negative if the coefficient was less than zero. The association between metabolic cluster and wound response score was evaluated using a 2-tailed Fisher exact test (conducted in SAS version 9.2).

Cell culture

Primary CAFs were isolated from breast tissue of patients undergoing breast surgery for primary invasive breast carcinoma at UNC Hospital. Tissue specimens were procured under an IRB-approved protocol (LCC 0913) by the Lineberger Cancer Center Tissue Procurement Facility and stored in 10 mL of Dulbecco's Modified Eagle's Media (DMEM)/F12 with 10% FBS on ice until processing (up to 6 hours). Tissue was minced and transferred to a 15-mL conical tube with 9 mL of suspension media: DMEM/F12 (GIBCO) supplemented with 10% FBS (GIBCO), 1% Pen/Strep (Invitrogen), 2.5 μg/mL Amphotericin B solution (Invitrogen), 300 U/mL collagenase (Sigma), and 100 U/mL hyaluronidas (Sigma). Collagenase digestion occurred overnight at 37°C, and the sample was then centrifuged for 30 seconds at 100 × g. A top layer of hydrolyzed fat was discarded and supernatant was centrifuged at 200 × g for 3 minutes. Supernatant was transferred to a new tube and centrifuged at 400 × g for 5 minutes. The supernatant was discarded, and the remaining fibroblast pellet was resuspended in 7 mL of suspension media, as described earlier, and transferred to a T25 flask. Cells were grown at 37°C in a 5% CO_2, with media changed every 3 to 5 days and split into a T75 at 80% confluency.

SUM149 (basal-like) and MCF7 (luminal) breast cancer cell lines were obtained from American Type Culture

Downloaded from http://aacrjournals.org/clincancerres/article-pdf/19/3/571/2296963/571.pdf by guest on 24 August 2022

Collection (30). Cell lines were maintained 37°C and 5% CO_2 in DMEM/F12 supplemented with 10% FBS and 50 units/mL penicillin/streptomycin. Cell lines were tested for mycoplasma by the Tissue Culture Facility at Lineberger Cancer Center.

Cocultures

Two types of cocultures were conducted to model the tumor metabolic microenvironment. First, we conducted *direct cocultures*, defined as a coculture where the 2 cell types are grown in physical contact, in the same well. Direct cocultures were used for all of the glucose assays plated at a physiologically relevant 1:2 ratio of cancer cells to fibroblasts in 24-well plates and were maintained for 96 hours, changing the media at 48 hours, before assays were conducted. Second, we conducted *indirect cocultures* or *transwell cultures*, where fibroblasts and cancer cells are grown separated by a membrane but in contact via soluble factors. Indirect cocultures were solely used to calculate individual cell growth rates for interacting stromal and epithelial cells. These studies were conducted by seeding 1 of the 2 cell types on the insert layer of Corning Transwell plates with 0.4-mm pore polycarbonate membranes, whereas the other cell type was grown in the bottom of the well. At 96 hours, 48 hours after media change, cells were harvested from top and bottom wells and counted using a Coulter Counter (Beckman Coulter, Inc.) to determine the ratio of cells. Identical starting stromal–epithelial ratios and analysis time points were used for both direct and indirect cultures. Two luminal and 1 basal-like primary CAF cell lines were used for all *in vitro* experiments, and all experiments were repeated in triplicate. For hepatocyte growth factor (HGF) inhibition, cells were treated with 0.5 μg/mL of anti-HGF antibody (Abcam) at time of plating, and media were not changed during the course of the experiment (48 hours).

Glucose uptake assay

Cells were plated for direct coculture at 1.0×10^5 epithelial cells per well and 2.0×10^5 fibroblasts/well into 24-well plates and allowed to grow for 96 hours, with media changed at 48 hours. Cells that were treated with anti-HGF antibody or sham were assayed at 48 hours. The cells were washed twice with 0.5 mL 37°C 1× PBS and then incubated for 10 minutes at 37°C in 0.5 mL/well KRH buffer (136 mmol/L NaCl, 4.7 mmol/L KCl, 1.25 mmol/L $CaCl_2$, 1.25 mmol/L $MgSO_4$, 10 mmol/L HEPES, pH 7.4) with 0.5 μCi/mL [^{3}H]2-deoxy-D-glucose (PerkinElmer). Cells were washed twice with 0.5 mL iced 1× PBS with 20 mmol/L D-glucose and then lysed in 0.5 mL lysis buffer (0.025% SDS, 1% Triton X-100 in 1× PBS). Lysates were centrifuged at 20,000 × *g* for 5 minutes at 4°C, and the protein concentration was determined with a Bicinchoninic Acid (BCA) assay (Thermo Fisher Scientific). The rest of the lysate was then added to a scintillation vial filled with 4.5 mL EcoScint H (National Diagnostics) for scintillation counting. Because cell composition changes during the time of coculture (due to different growth rates for cancer cells and fibroblasts), expected metabolic responses for cocultures were computed using cell numbers at time of measurement and using measured activity levels. For each of *n* cocultures, the following formula was used to calculate expected metabolic activity level:

$$m_{\text{n coculture}} = \{(a \cdot m_{\text{epi mono}}) + ((1 - a) \cdot m_{\text{caf mono}})\}$$

where m = metabolic activity and a = fraction of epithelial cells as estimated by cell counts for both cell types at a given time point after the start of coculture. Expected activity computed by this formula was compared with observed activity, and fold change was computed as a function of expected over observed metabolic activity. Statistical analyses of these data were conducted with 2-tailed *t* tests (e.g., all MCF7 cocultures vs. all SUM149 cocultures, or all LCAF cocultures vs. BCAF cocultures, etc.).

Glucose oxidation/glycogen synthesis

Cells were plated for direct coculture at 1.0×10^5 epithelial cells per well and 2.0×10^5 fibroblasts per well into 24-well plates and allowed to grow for 96 hours, with media changed at 48 hours. The cells were washed twice with 0.5 mL 37°C 1× PBS and then incubated for 120 minutes at 37°C in 0.5 mL/well KRH buffer (136 mmol/L NaCl, 4.7 mmol/L KCl, 1.25 mmol/L $CaCl_2$, 1.25 mmol/L $MgSO_4$, 10 mmol/L HEPES, pH 7.4) with 2 μCi/mL [^{14}C] uniformly labeled D-glucose (PerkinElmer). Following incubation, 400 μL of KRH media from each well was placed into the upper well of an oxidation plate with 200 μL 1 mol/L NaOH in the lower well. The oxidation plate was sealed with a gasket and lid and the media well acidified by injecting 100 μL 70% perchloric acid. The oxidation plate was placed on an orbital shaker for 1 hour and then 150 μL of the NaOH from each well was placed into a scintillation tube with 4.5 mL EcoScint H for scintillation counting. The data are expressed as DPM/mg of protein/minute. Cells from this assay were washed twice with 0.5 mL iced 1× PBS with 20 mmol/L D-glucose and then lysed in 0.5 mL lysis buffer (30% KOH saturated with Na_2SO_4). Lysates were heated to 95°C for 10 minutes and centrifuged at 20,000 × *g* for 5 minutes at 4°C. The protein concentration was determined with a BCA assay (Thermo Fisher Scientific). To the remaining lysate, an equal volume of 100% ethanol was added to precipitate glycogen and samples stored at −20°C overnight. Samples were centrifuged at 20,000 × *g* for 5 minutes at 4°C and the supernatant removed. The pellets were washed in 1 mL of 70% ethanol and centrifuged at 20,000 × *g* for 5 minutes at 4°C. Supernatants were removed and pellets air-dried overnight. Pellets were then resuspended in 0.5 mL water and transferred to a scintillation vial with 4.5 mL EcoScint H for scintillation counting. The data are expressed as DPM/mg of protein/h fold change of observed/expected. For each of these cocultures, the expected activities of glucose oxidation and glycogen synthesis pathways were computed as described earlier and used to compute fold change relative to expected. Statistical analyses of these data were conducted as described earlier for glucose uptake.

Downloaded from http://aacrjournals.org/clincancerres/article-pdf/19/3/571/2296963/571.pdf by guest on 24 August 2022

Lactate assay

Cells were plated at 1.0×10^5 epithelial cells per well and 2.0×10^5 fibroblasts per well into 24-well plates and allowed to grow for 48 hours, media were collected and stored in aliquots at −80°C and assayed for lactate content. Briefly, fresh NAD+ was added to assay buffer (175 mmol/L hydrazine sulfate, 68 mmol/L glycine, 2.9 mmol/L EDTA, 11.3 mmol/L NAD+, pH 9.5) just before assay. In a 96-well plate, 200 μL of assay buffer and 40 μL of lactate standard or media sample were combined in each well. The plate was then preread at 340 nm followed by the addition of 1U of lactate dehydrogenase in a 10 μL volume of water. The plate was mixed and read at 340 nm. The lactate concentration in each sample was determined from the standard curve. Computed expected levels of lactate were conducted as described for other metabolic assays earlier. Statistical analyses of these data were conducted as described earlier for glucose uptake.

Western blot analysis

Cells were harvested from culture, and protein was isolated and quantitated. Lysates were denatured by boiling with β-mercaptoethanol, and 30 μg of protein was electrophoresed on a 4% to 20% Tris-HCl Criterion precast gel (Bio-Rad) and transferred to a Hybond-P membrane (Amersham Biosciences) by electroblotting. The blots were probed with antibodies against the GLUT1 (Abcam) and β-actin (Cell signaling). Blots were washed 3 times with Tris-buffered saline supplemented with 0.1% Tween and then were probed with ECL anti-mouse IgG horseradish peroxidase (HRP)-linked whole antibody from rabbit (Amersham-GE Healthscience). Blots were rewashed, and detection was by enhanced chemiluminescence Western blotting detection system (Amersham-GE Healthcare). Relative GLUT1 protein concentration was quantified using ImageJ software, pixel intensity was used to measure the protein band of GLUT1 and divided by the intensity of the β-actin band.

Analysis of cytokine expression in conditioned media

Conditioned media from direct 1:1 cocultures (48 hours) was analyzed on a RayBio Human Cytokine Antibody Array 5 (80; Raybiotech) designed to detect 80 cytokines and chemokines. These glass arrays were used according to manufacturer protocol to measure cytokine and chemokine expression in the conditioned media from direct cocultures. Briefly, slides were blocked by incubation with blocking buffer at room temperature for 30 minutes and incubated with 100 μL of the sample at room temperature for 90 minutes. Membranes were washed and incubated with biotin-conjugated antibodies overnight at 4°C. Finally, the membranes were washed and incubated with fluorescent dye–conjugated streptavidin at room temperature for 2 hours. After final washing, slides were dried by centrifugation at 1,000 rpm for 3 minutes. Fluorescent signal was detected on a laser scanner using a cy3 (green) channel (excitation frequency 532 nm). Data for each cytokine were normalized to positive controls on the same slide to estimate relative protein expression. Each monoculture or direct coculture was analyzed in duplicate.

cDNA synthesis and qPCR analysis

RNA was isolated from cultured cells using RNeasy Mini kit (Qiagen) following manufacturers' instructions. One microgram of total RNA was reverse transcribed into cDNA using iScript cDNA synthesis kit (Bio-Rad). Quantitative PCR (qPCR) was carried out with a dilution of cDNA equivalent to 100 ng RNA in 18 μL of master mix [10 μL SsoFast 2X Probes Supermix (Bio-Rad), 0.5 μL 18S-VIC, and 0.5 μL gene-specific Assay-On-Demand-FAM (Applied Biosystems), 7 μL water] was used in each well of the qPCR 96-well plate. The following primer/probe sets (Applied Biosystems) were used: *GLUT1*, *18S*. Amplification conditions were as follows: 1 cycle of 95°C for 1 minute; 40 cycles of 95°C for 5 seconds, 60°C for 20 seconds. The best linear fit equation generated by the amplicon standard curve was used to determine the number of copies of *GLUT1* in the cDNA generated. Relative transporter expression was normalized to the expression of *18s*. Statistical analyses of these data were conducted with a 2-tailed *t* test (e.g., cocultures vs. monocultures, or cocultures with and without HGF antibody).

Results

Evidence of two distinct metabolic clusters

To identify metabolic subgroups of tumors, unsupervised hierarchical clustering was conducted on 379 metabolites across 31 breast tumor and 6 normal breast tissue samples. Patient characteristics for these 37 patients are described in Table 1. Two main clusters resulted (dendrogram shown in Fig. 1A and heatmap shown in Fig. 1C), one of which (cluster 1) was primarily normal tissue and less aggressive tumors (90% of luminal A tumors; 100% of normal breast tissues; Fig. 1B, colored boxes). The other cluster (cluster 2) was enriched for more aggressive tumor subtypes and metastatic tumors (60% of basal-like tumors; 66.7% of luminal B tumors; 100% of metastases). Cluster 2 tumors had significantly larger tumor size ($P = 0.047$) than those in cluster 1. While associations were not statistically significant, cluster 2 tumors were also substantially more likely to be ER-negative (Fig. 1B, gray scale boxes) and have poorly differentiated tumor grade.

Given the importance of stromal cells in altering glucose metabolism of cancer cells in previous literature (10, 31, 32), we hypothesized that metabolite subtypes would correlate with stroma-driven gene expression in the human tissue specimens. Using a published wound response signature identified in cancer-adjacent stroma-rich breast tissue when compared with breast tissue from reduction mammoplasty (25), we observed an association between metabolic cluster and wound response, with a higher percentage of tumors in cluster 2 (the more aggressive metabolic group) expressing activated wound response signature (Fig. 1D, $P = 0.054$). Of the tumors in cluster 1, 39% were positively correlated with the wound response

Downloaded from http://aacrjournals.org/clincancerres/article-pdf/19/3/571/2296963/571.pdf by guest on 24 August 2022

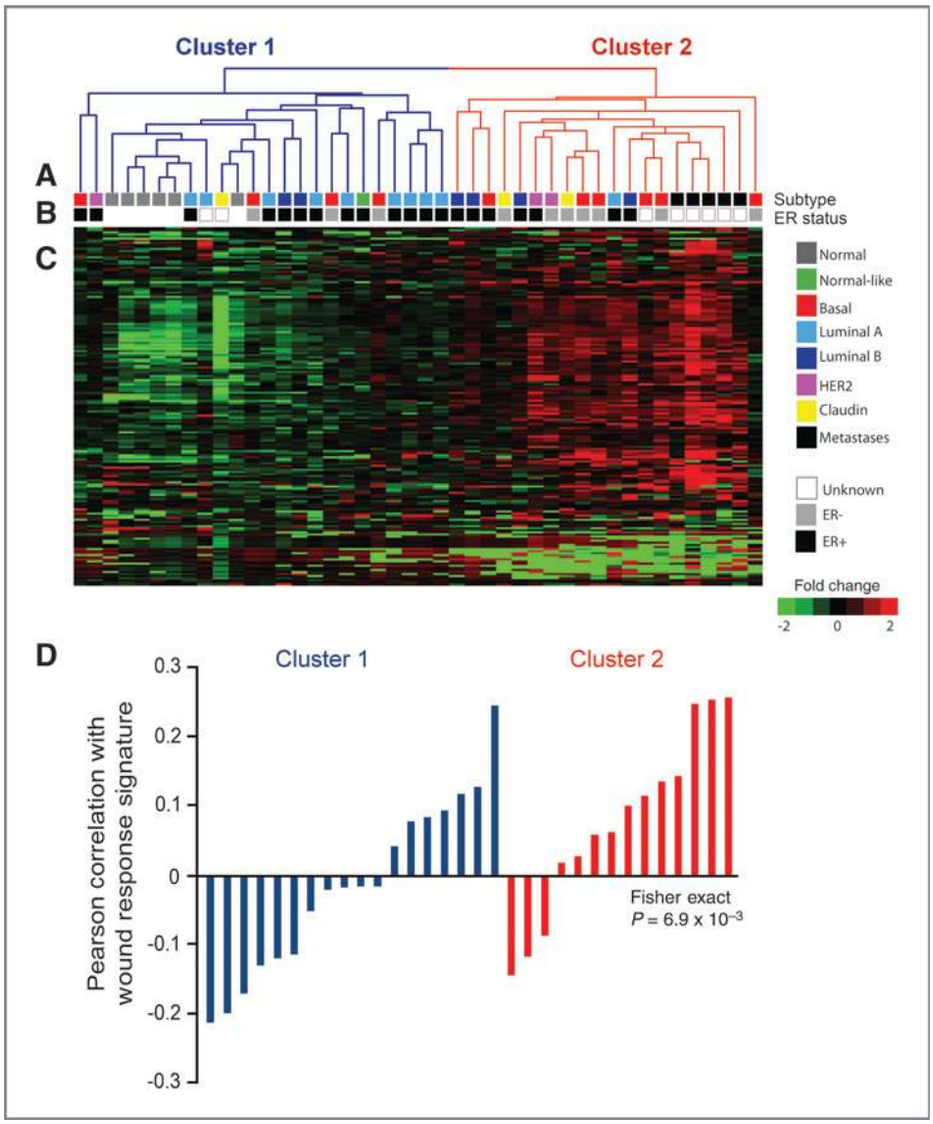

Figure 1. Unsupervised cluster analysis of 379 metabolites resulted in 2 main clusters (clusters 1 and 2; A). Cluster 1 (blue lines in dendrogram) included less aggressive tumor types or normal breast samples, whereas cluster 2 (red lines in dendrogram) included more aggressive tumors and metastases (B; colored bars). Clusters of metabolites in the heatmap (C) implicated hallmark Warburg phenotypes in aggressive tumors: elevated levels of amino acids, nucleic acids, and decreased steady state levels of sugars/carbohydrates and citric acid cycle metabolites. Pearson correlation of tumor gene expression with a previously published wound response signature shows a role for stromal activation in cluster 2; that is, metabolic class was strongly correlated with expression of an *in vivo* wound response signature (ref. 25; D).

signature, whereas 79% of tumors in cluster 2 were positively correlated with the signature. Interestingly, the association between metabolic subtype and wound response signature was stronger than the association with either ER status or breast tumor subtype (Table 1).

Pathway-driven metabolic phenotypes in breast tumors

Four well-defined groups of metabolites defined the differences between metabolic clusters: amino acids, sugars, nucleic acids, and metabolites involved in the tricarboxylic citric acid (TCA) cycle. Principal component analysis (PCA) using metabolites in each of these 4 metabolite classes separated the cluster 1 and 2 tumors and delineated normal from metastatic samples (Fig. 2). The association between metabolite levels and metabolite cluster was strongest for amino acids (Fig. 2A; PC1, 85.7%; PC2 4.3%), followed by nucleic acids (Fig. 2B; PC1, 51.6%; PC2, 24.3%), TCA cycle (Fig. 2C; PC1, 54.2%; PC2, 17.2%), and carbohydrates/sugars (Fig. 2D; PC1, 32.8%; PC2, 13.6%), suggesting the relative importance of these types of metabolites in driving clustering and aggressive tumor subtype. Considering individual metabolites in each of these 4 categories, there were 19 amino acids that increased between normal samples and cluster 1 and between cluster 1 and non-metastatic tumors in cluster 2 (Table 2). Many of these metabolites increased further in metastatic tumors from different sites (skin, lung, liver, or brain). Several individual metabolites showed a trend from normal to cluster 1 tumors to cluster 2 non-metastatic tumors, including glucose (decrease), glucose-6-phosphate (increase), lactate (increase), and ribulose-5-phosphate (increase). Malic acid and fumaric acid, both metabolites in the TCA cycle, increased from normal to cluster 1 tumors to cluster 2 non-metastatic tumors, inversely proportional to citric acid levels. In summary, many metabolites that are crucial for glucose metabolism and

Downloaded from http://aacrjournals.org/clincancerres/article-pdf/19/3/571/2296963/571.pdf by guest on 24 August 2022

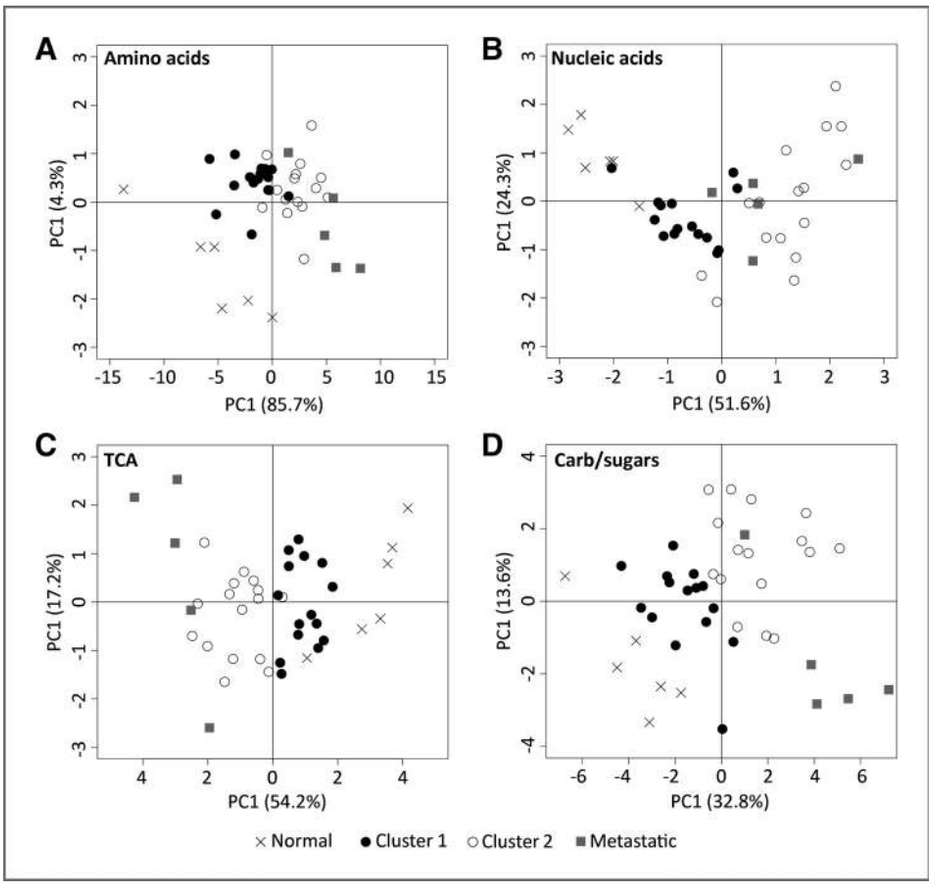

Figure 2. PCA reveals a separation of tumor phenotype by key metabolite groups. Four classes of metabolites—(A) amino acids, (B) nucleic acids, (C) TCA cycle metabolites, and (D) carbohydrates/sugars—distinguish normal breast tissue samples, tumors in the less aggressive metabolite cluster (cluster 1), tumors in the more aggressive metabolite cluster (cluster 2), and metastatic tumors.

the citric acid cycle were present at lower or higher levels in the more aggressive tumor cluster (cluster 2) than in cluster 1. A diagram illustrating the pathways affected by this metabolic shift is presented in Fig. 3.

Metabolic processes indicate stroma-influenced Warburg effect

Previous experimental studies focused on specific metabolic hallmarks of Warburg phenomenon recently identified a reverse Warburg effect, where stromal cells act as important drivers of the metabolic phenotype of cancers (10, 11, 14, 15, 33). Given this previous literature and the correlation between metabolic phenotype and wound response genomic signature, we conducted cocultures that modeled basal-like and luminal metabolic microenvironments to assess whether fibroblast characteristics, cancer cell characteristics, or interactions between the 2 were important in tumor metabolism. Basal-like microenvironments were modeled with SUM149 basal-like breast cancer cells and with basal-like CAFs (BCAFs). Luminal microenvironments were modeled with MCF7 luminal breast cancer cells and luminal CAFs (LCAFs). Results showed a complex interplay of stromal and epithelial cells in determining metabolic phenotype.

Consistent with the observation that more aggressive subtypes have more extreme metabolic phenotypes, SUM149 (basal-like) cells displayed higher glucose uptake than MCF7 (luminal) cells in monoculture (Supplementary Fig. S1A). However, SUM149 cells had even greater glucose uptake when grown with BCAFs (Fig. 4A), showing a 2.9-fold increase in observed relative to expected ($P < 0.001$). BCAFs also increased MCF7 glucose uptake (1.9-fold higher than expected, $P = 0.001$). In contrast, LCAFs suppressed glucose uptake in MCF7 cocultures but had no effect in coculture with SUM149 cells. Overall, BCAF cocultures had a 2.8-fold increase in glucose uptake when compared to LCAF cocultures ($P = 0.04$).

Once glucose is taken up, utilization includes glucose oxidation, glycogen synthesis, and lactate production, which are endpoints of oxidative metabolism, storage, and glycolysis, respectively. Basal-like cells had higher glucose oxidation in monoculture (Supplementary Fig. S1). However, glucose oxidation was suppressed in all luminal coculture conditions (MCF7 cells or LCAFs present, Fig. 4B). Increased glucose oxidation among SUM149 cells occurred only when these cells were cocultured with BCAFs (2.1-fold higher glucose oxidation than SUM149s with LCAFs, $P < 0.001$). This is interesting, suggesting that both stromal and epithelial factors contribute to glucose oxidation.

Glucose oxidation in the cell is balanced by non-oxidative glucose utilization, including glycogen synthesis. Stored cellular glycogen can promote cell survival in conditions of hypoxia (33). Glycogen synthesis was increased in all cocultures relative to monocultures (Fig. 4C); however, the

Downloaded from http://aacrjournals.org/clincancerres/article-pdf/19/3/571/2296963/571.pdf by guest on 24 August 2022

Table 2. Mean metabolite levels and trend for four key groups

	Mean value					
Metabolite[a]	**Normal**	**Cluster 1**	**Cluster 2**	**Mets**	**β Value (SE)[b]**	**P_{trend}[c]**
Amino acids						
Alanine	22.2	23.3	24.9	26.1	1.36 (0.12)	<0.001
Proline	21.4	22.7	24.2	25.3	1.36 (0.15)	<0.001
Glycine	21.8	23.8	25.5	26.7	1.67 (0.16)	<0.001
Histidine	18.7	20.0	21.4	22.3	1.27 (0.16)	<0.001
Leucine	21.4	22.5	23.8	24.8	1.18 (0.15)	<0.001
Isoleucine	20.3	20.9	22.3	23.2	1.04 (0.17)	<0.001
Valine	21.0	21.9	23.1	24.0	1.05 (0.14)	<0.001
Threonine	19.4	20.6	22.0	23.1	1.30 (0.16)	<0.001
Methionine	20.3	21.1	22.4	23.1	1.00 (0.14)	<0.001
Serine	20.4	21.7	23.0	23.7	1.18 (0.15)	<0.001
Phenylalanine	22.9	23.4	24.5	25.1	0.82 (0.13)	<0.001
Tyrosine	21.8	22.5	23.6	24.3	0.88 (0.13)	<0.001
Lysine	19.0	20.2	21.0	21.7	0.90 (0.13)	<0.001
Tryptophan	21.4	21.9	22.9	23.8	0.83 (0.13)	<0.001
Arginine	18.4	19.1	19.8	20.4	0.68 (0.13)	<0.001
Asparagine	17.2	18.8	19.6	20.3	0.97 (0.15)	<0.001
Glutamine	20.8	21.7	22.5	23.5	0.87 (0.17)	<0.001
Taurine	16.2	18.7	19.2	19.1	0.90 (0.15)	<0.001
Ornithine	17.0	17.3	17.8	20.0	0.86 (0.18)	<0.001
Carbohydrates/sugars						
Lactate	23.7	25.4	27.0	27.9	1.49 (0.15)	<0.001
Mannose-6-phosphate	14.4	15.4	17.4	17.8	1.34 (0.18)	<0.001
N-acetylglucosamine 6-phosphate	14.8	15.5	16.9	17.3	0.95 (0.13)	<0.001
Isobar: ribulose 5-phosphate, xylulose 5-phosphate	15.2	15.4	16.9	16.7	0.76 (0.19)	<0.001
Fructose-6-phosphate	15.1	16.6	18.2	18.7	1.31 (0.17)	<0.001
N-acetylneuraminate	15.8	16.2	17.5	18.5	0.98 (0.16)	<0.001
Glucose-6-phosphate	15.9	18.2	19.9	20.5	1.58 (0.21)	<0.001
Erythronate	14.5	15.4	16.8	18.8	1.43 (0.19)	<0.001
UDP-*N*-acetylgalactosamine	16.0	18.9	20.9	21.3	1.87 (0.30)	<0.001
Glucose	22.4	20.8	19.5	20.5	−0.84 (0.27)	0.004
Glycerate	15.8	15.9	16.4	17.4	0.51 (0.11)	<0.001
Xylitol	17.6	17.8	16.9	18.1	−0.11 (0.19)	0.564
Sedoheptulose-7-phosphate	14.1	13.2	14.2	14.1	0.23 (0.21)	0.273
Maltose	16.7	17.0	17.9	19.4	0.87 (0.23)	<0.001
1,5-Anhydroglucitol	17.7	17.7	18.5	18.7	0.41 (0.20)	0.040
Sorbitol	16.8	18.0	17.3	19.0	0.38 (0.23)	0.099
Fructose	17.6	16.2	16.6	18.6	0.29 (0.22)	0.204
3-Phosphoglycerate	16.2	16.7	17.2	18.0	0.57 (0.18)	0.004
Mannose	16.8	17.1	16.7	18.1	0.20 (0.19)	0.309
Mannitol	17.6	18.5	18.7	20.9	0.85 (0.27)	0.003
N-acetylmannosamine	17.1	18.0	17.9	17.6	0.13 (0.19)	0.485
Pyruvate	17.3	18.0	17.9	16.6	−0.15 (0.17)	0.391
Phosphoenolpyruvate	15.5	15.3	15.3	15.8	0.13 (0.13)	0.636
Nucleic acids						
Uracil	14.9	18.1	20.2	21.5	2.21 (0.20)	<0.001
Guanine	15.4	18.2	20.3	18.3	1.32 (0.28)	<0.001
Adenine	17.6	17.6	16.0	16.6	−0.64 (0.23)	0.010
Thymine	17.6	18.0	17.1	16.9	−0.38 (0.20)	0.059

(Continued on the following page)

Downloaded from http://aacrjournals.org/clincancerres/article-pdf/19/3/571/2296963/571.pdf by guest on 24 August 2022

Table 2. Mean metabolite levels and trend for four key groups (Cont'd)

	Mean value					
Metabolite[a]	**Normal**	**Cluster 1**	**Cluster 2**	**Mets**	**β Value (SE)[b]**	**P_{trend}[c]**
TCA cycle						
Phosphate	24.2	25.6	27.1	28.1	1.35 (0.10)	<0.001
Fumarate	15.3	16.9	18.8	19.1	1.44 (0.14)	<0.001
Malate	16.4	18.5	20.5	21.0	1.66 (0.17)	<0.001
α-Ketoglutarate	13.9	14.0	14.7	19.7	1.56 (0.26)	<0.001
Citrate	18.6	17.9	17.4	17.8	−0.35 (0.19)	0.082
Pyrophosphate (PPi)	18.9	19.9	20.1	20.4	0.47 (0.11)	<0.001
Succinate	15.7	15.8	16.1	18.0	0.016 (0.25)	0.016

[a]Data are reported as mean-normalized median-centered metabolite levels.
[b]β value (SE) corresponding to linear regression of metabolite level on an ordinal variable equal to 1 for normal, 2 for cluster 1, 3 for cluster 2, and 4 for metastases.
[c]P_{trend} column indicates statistical significance of the β value.

increase in glycogen synthesis was most noticeable among SUM149 cocultures.

Finally, we assessed lactate as a measure of anaerobic glycolysis. Lactate production was higher in basal-like cancer cells and CAFs than in luminal cells in monoculture (Supplementary Fig. S1A); however, all coculture models showed about a 1.5-fold higher-than-expected lactate production that was not subtype-driven (Supplementary Fig. S1B). Considering all of these metabolites, coculture of basal-like epithelial cells with basal-like fibroblasts revealed

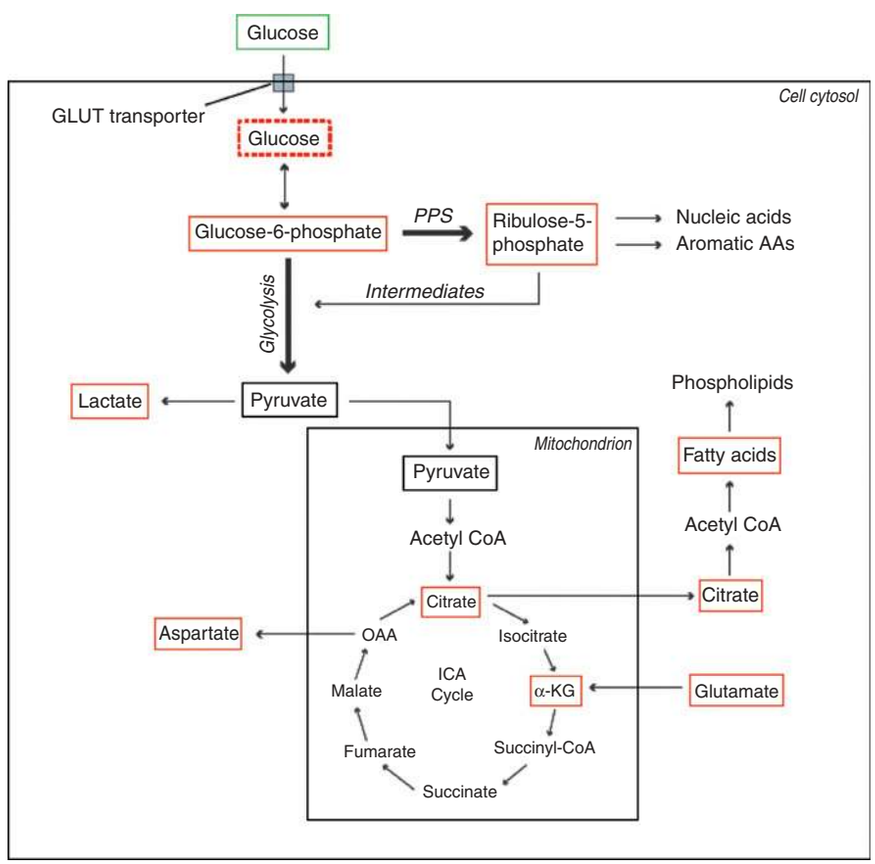

Figure 3. Schematic representing major metabolic pathways in the Warburg effect and their relative levels in distinct groups of breast tumors. Red boxes indicate an increase in metabolite levels in cluster 2 compared with the less aggressive cluster 1, whereas a green box indicates decreasing levels. The dotted red box indicates marginally increased metabolite levels. Glucose processing through glycolysis to pyruvate and lactate provides ATP, whereas the pentose phosphate shunt (PPS) generates key intermediates in nucleotide biosynthesis. Glucose-derived citrate is exported to the cytosol to contribute to lipid production. Glutamine is converted into glutamate and is transported to the mitochondria where it is deaminated to generate α-ketoglutarate, an intermediate in the TCA cycle. Aromatic AA, aromatic amino acids; OAA, oxaloacetate; acetyl CoA, acetyl coenzyme A; and succinyl CoA, succinyl coenzyme A.

Downloaded from http://aacrjournals.org/clincancerres/article-pdf/19/3/571/2296963/571.pdf by guest on 24 August 2022

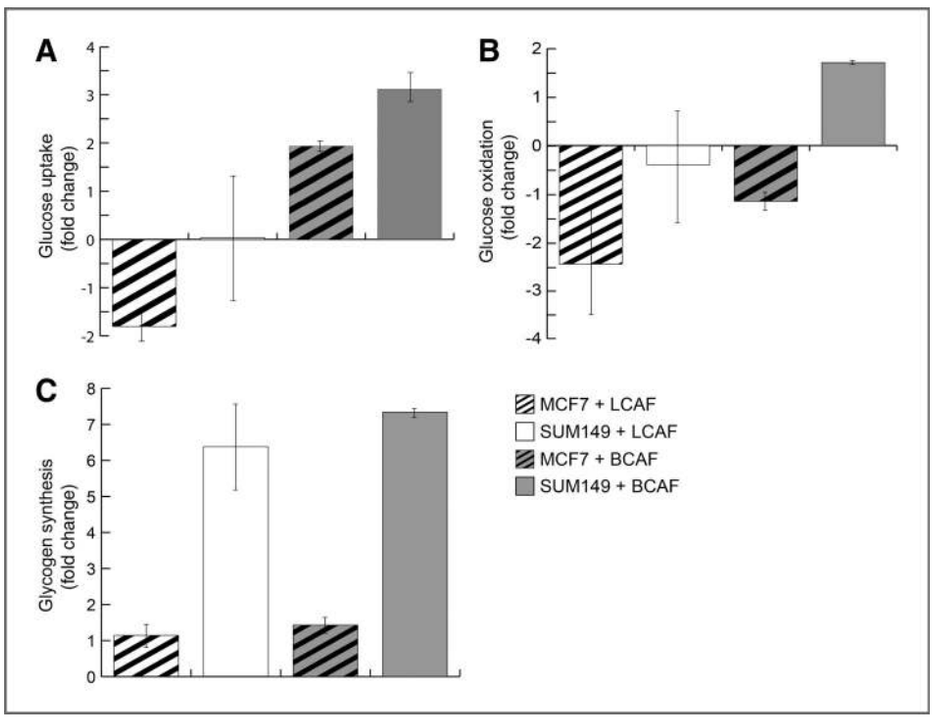

Figure 4. Glucose metabolism is regulated by aggressiveness of both tumor and stroma. Glucose uptake is increased by BCAFs. SUM149 cells had higher levels of glucose uptake than MCF7 cells in coculture regardless of fibroblast type (A). Glucose oxidation was suppressed in luminal cocultures (MCF7 or LCAF), whereas SUM149 cells cocultured with BCAFs had increased glucose oxidation (B). Finally, analysis of glycogen synthesis (C) revealed an increase in all coculture conditions relative to monocultures, with the strongest fold change among basal-like breast cancer cells (SUM149). All fold change values are expressed relative to the expected levels based on coculture composition and monoculture metabolism, as described in Materials and Methods.

the strongest phenotype of elevated glucose metabolism including glycolysis, oxidation, and storage.

Glucose uptake regulated by tumor–stromal interactions between GLUT1 and HGF

Given the importance of stromal cells in altering glucose metabolism of cancer cells in previous literature (10, 32, 33) and our coculture data, we hypothesized that the expression of glucose transporters may be regulated by tumor–stromal interactions. GLUT1–4 are class I integral membrane proteins responsible for the transport of glucose. We focused on GLUT1 because it is responsible for basal levels of glucose uptake in all cells and glucose levels inversely regulate its expression (34). GLUT1 has also been shown to be the predominant glucose transporter in human breast carcinomas and mouse mammary carcinomas (35, 36). GLUT1 protein levels were higher in the more aggressive SUM149 monocultures than in MCF7 monocultures (Fig. 5A). Coculture conditions further increased GLUT1 protein levels in both cell types, showing a role for stroma in the regulation of glucose metabolism (Fig. 5A). To identify soluble factors and specific pathways regulating this change in GLUT1, cytokine protein arrays were conducted. These results indicated significantly higher levels of HGF in coculture conditions (Fig. 5B). Consistent with previous data in muscle (37), we hypothesized that HGF was playing a regulatory role in *GLUT1* expression. We were able to completely block *GLUT1* RNA expression by inhibiting HGF levels in the media, confirming our hypothesis (Fig. 5C). To further confirm this mechanism and its downstream effects on metabolism, we compared levels of glucose uptake in stromal–epithelial cocultures with and without HGF inhibition. Our results show 65.6% decrease in glucose uptake ($P = 0.055$) with HGF inhibition in SUM149:RMF cocultures (Fig. 5D).

Discussion

Gillies and Gatenby (38) have argued that adaptations to resource scarcity are fundamental in the evolution of carcinogenesis and have shown that a variety of pathways dysregulate aerobic glycolysis in tumors (39). Consistent with metabolic adaptation during carcinogenesis, metabolite profiles can distinguish cancer from non-cancer (40). However, while it has been increasingly recognized that cancers evolve into distinct breast cancer subtypes, few studies have evaluated evolution of metabolic differences between breast cancer subtypes (39, 41–44). Our study shows that tumors differ from normal samples in their metabolomic profiles but extended this to describe metabolomic heterogeneity within tumors. High-resolution quantitative profiling of metabolites from normal and tumor tissue identified 2 metabolic subgroups that were associated with aggressive tumor characteristics. Interestingly, although these metabolic subtypes did not strongly correlate with established PAM50 or claudin-low tumor gene expression subtypes. While larger studies are warranted to allow better powered analysis of how intrinsic subtype affects metabolism, an important next step was to understand whether other genomic signals correlate with metabolic subgroups.

We hypothesized that interactions between tumor epithelium and stroma can be detected in genomic data and that these interactions contribute to the evolution of distinct metabolic microenvironments. Previous genomic studies

Downloaded from http://aacrjournals.org/clincancerres/article-pdf/19/3/571/2296963/571.pdf by guest on 24 August 2022

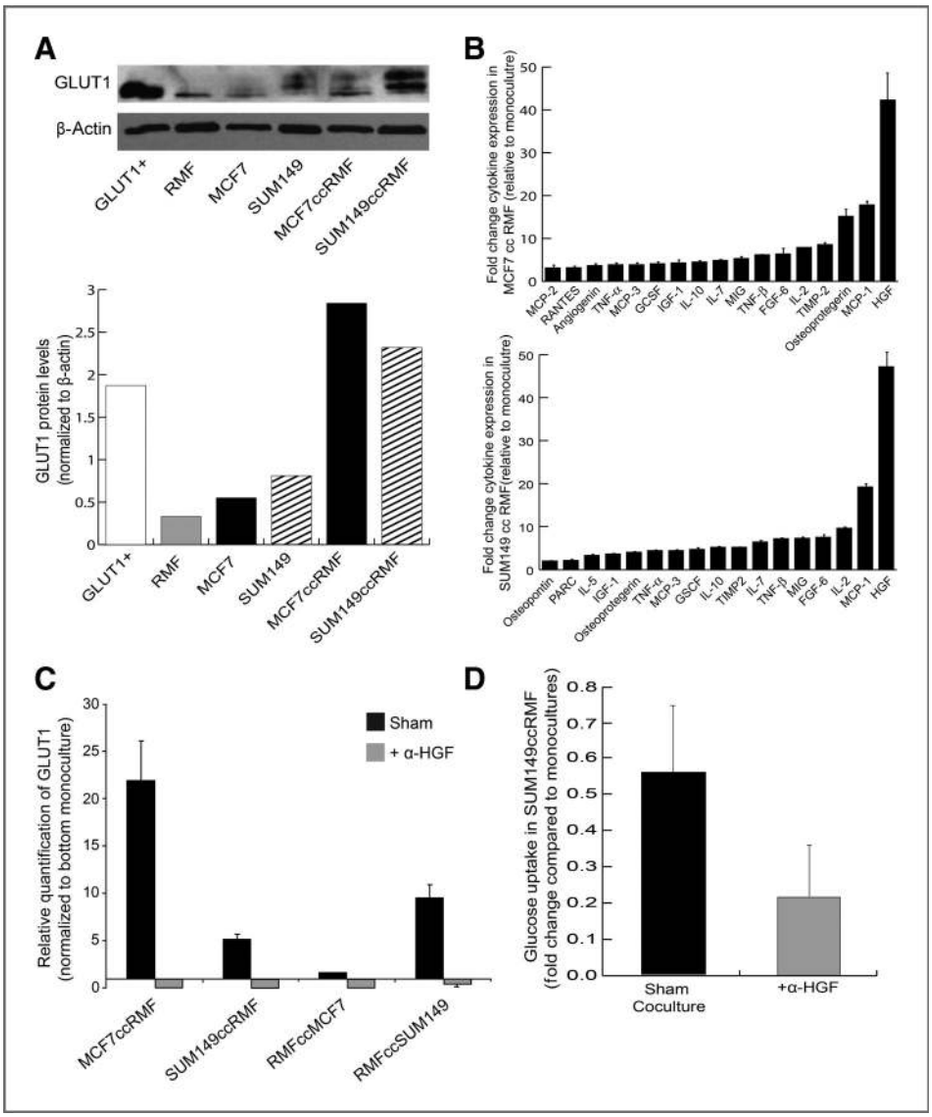

Figure 5. HGF-dependent regulation of GLUT1 expression in breast cancer. GLUT1 protein expression is elevated in coculture (cc) models compared to monocultures of RMF, MCF7, and SUM149 cells (A). Cytokine arrays identify HGF as a key factor significantly induced in coculture for both luminal (MCF7) and basal-like (SUM149) breast cancer cells (B), when blocked using an HGF-neutralizing antibody (α-HGF), the *GLUT1* receptor is inhibited at the RNA level (C). Levels of glucose uptake decrease by 66% ($P = 0.055$) in SUM149 cells when HGF is inhibited using antibody (D).

have emphasized the importance of host–tumor interactions in progression (45), suggesting possible pathways to test in association with metabolomic subtype. From microarray studies, a wound response is tumor promoting in the presence of initiated cells (46, 47) and wound response gene signatures are prevalent in tumor-adjacent, stroma-enriched tissue (25). Thus, we tested an *in vivo* wound response signature and found its expression to be strongly associated with metabolic subtype. These results show that integrated analyses of metabolite and gene expression data can identify phenotypically distinct groups of breast cancers.

Other recent articles have conducted integrated analyses of metabolomics and gene expression datasets, emphasizing identification of genes associated with individual metabolite levels or identification of metabolic phenotypes associated with specific tumor characteristics (48–51). A large study of metabolite profiles across 289 tumor samples identified groups of tumors corresponding to hormone receptor status and grade, however, that study did not seek to identify associated genomic changes beyond these tumor characteristics (49). Borgan and colleagues analyzed metabolite profiles of 46 mostly luminal A breast cancers (48) and linked metabolic heterogeneity within the luminal A breast cancers to gene expression differences, including differences in extracellular matrix (ECM) genes. Their observation of the importance of ECM genes in metabolism is consistent with our finding that metabolism was strongly correlated with stromal signature and stromal–epithelial interactions. Also consistent with our findings, Borgan and colleagues noted heterogeneity within the luminal A subtype, showing that intrinsic subtype alone does not determine metabolic phenotype (48). In our study, we aimed to include a more diverse sample set with 6 different subtypes of breast cancer and an approximately even distribution of ER^+ and ER^- tumors. Our power to conduct comprehensive assessments

Downloaded from http://aacrjournals.org/clincancerres/article-pdf/19/3/571/2296963/571.pdf by guest on 24 August 2022

of subtype-specific changes was limited due to sample size, but our results do suggest heterogeneity of response within classes defined by tumor subtype.

Few integrated, observational studies of gene expression and metabolomics data, including our own dataset, have been of sufficient size to evaluate both tumor and stromal characteristics. To address this limitation, we combined our tissue-based observations with well-established cell culture–based models that mimic the tumor interactions with microenvironment (5) to confirm the pathway changes seen in our gene expression and metabolomics data. While we were unable to measure all metabolites, we selected the metabolism of glucose for more focused investigation because it is central to many of the Warburg-like changes observed in the full metabolic profile. Our results show that metabolic phenotype is a complex interplay between tumor characteristics and the surrounding stromal biology. Basal-like breast cancer epithelial cells more readily take up glucose from surrounding tissue than luminal breast cancer cells. Furthermore, basal-like CAFs also stimulate marked increases in glucose uptake, even in luminal breast cancer cells. Conversely, luminal CAFs produce no change or can slightly decrease glucose uptake and oxidation in basal-like breast cancer cells. Glucose oxidation depended on both stromal and epithelial characteristics, whereas glycogen synthesis appears to be less sensitive to the differences between luminal CAFs and basal-like CAFs, correlating most strongly with epithelial cell content. This latter pattern of metabolite production in coculture suggests an acquired capability—increased glycogen storage in response to microenvironmental signals—and raises the question as to whether increased glycogen synthesis is a hallmark of basal-like breast cancers.

While primary CAFs used in this study show that there is interindividual variation in the effect of CAFs, to establish central trends for basal-like versus luminal stroma will require greater numbers of cell lines. However, these results underscore the importance of understanding variation in tumor stroma. Characteristics of fibroblasts, such as aging or senescence phenotypes, can also alter metabolism as shown in recent studies (52). Our results confirm that understanding which metabolites are sensitive to stromal factors and which are dominated by epithelial characteristics is necessary if metabolic processes are to be targeted for cancer treatment or prevention.

Future metabolic-targeted treatment demands understanding of not just the metabolomics phenotypes but the genomic signals/pathways that drive these phenotypes. We conducted cytokine arrays to identify factors induced in coculture that could explain the shift to greater glucose uptake. Having observed large fold changes in HGF secretion, we conducted a literature search that suggested *GLUT1* expression is downstream of HGF-cMET signaling in liver and muscle (53, 54). Therefore, we hypothesized that the same pathway may be active in breast cancer. Previous literature shows a role for HGF/cMET in breast cancer aggressiveness. MET receptor protein tyrosine kinase regulates cell motility and invasion (55, 56) and is stimulated by HGF (57, 58). Together, the HGF-MET pathway has been shown to regulate stromal–epithelial interactions in multiple cancers (59–63). In breast cancer, HGF/c-MET signaling promotes tumorigenesis (64), increases metastasis (65, 66), and mediates drug resistance in most aggressive breast cancers (67–69). Our results show that HGF regulates *GLUT1* expression, which in turn regulates glucose uptake. Inhibition of exogenous HGF completely blocks *GLUT1* expression and decreases glucose uptake. Given the success of small-molecule inhibitors of c-MET in the clinic, the HGF/c-MET pathway may also be a target for the regulation of tumor cell metabolism.

In summary, reciprocal interactions between cancer epithelial cells and the surrounding microenvironment have an established impact on tumor growth (5, 6, 46) and a broad range of other metabolic and signaling processes (26, 43, 70). Previous studies by Castello-Cros et al. have shown extensive evidence *in vitro* for the stromal role in Warburg metabolism through matrix remodeling (2), stromal autophagy (11), and stromal–epithelial lactate exchange (71). Our results further show that both fibroblast and epithelial characteristics modulate specific metabolic phenotypes *in vitro* and pairs one of these changes, glucose uptake, with specific targetable gene expression changes (HGF/*GLUT1*). This study shows that integration of multiple data types in human tumor studies, together with *in vitro* experimental studies that dissect heterotypic interactions, can yield important advances in understanding the complex metabolic and genomic interactions during tumor evolution.

Disclosure of Potential Conflicts of Interest

No potential conflicts of interest were disclosed.

Authors' Contributions

Conception and design: H.A. Brauer, C.M. Perou, M.A. Troester
Development of methodology: H.A. Brauer
Acquisition of data (provided animals, acquired and managed patients, provided facilities, etc.): L. Makowski, P. Casbas-Hernandez, L.J. Lang, A.J. Freemerman, C.M. Perou
Analysis and interpretation of data (e.g., statistical analysis, biostatistics, computational analysis): H.A. Brauer, L. Makowski, K.A. Hoadley, L.J. Lang, E. Romàn-Pèrez, M. D'Arcy, C.M. Perou, M.A. Troester
Writing, review, and/or revision of the manuscript: H.A. Brauer, L. Makowski, K.A. Hoadley, L.J. Lang, C.M. Perou, M.A. Troester
Administrative, technical, or material support (i.e., reporting or organizing data, constructing databases): L.J. Lang, M. D'Arcy
Study supervision: M.A. Troester

Grant Support

The project was funded by the National Institutes of Environmental Health Sciences and NCI via Breast Cancer and the Environment Research Program (BCERP) U01-ES019472 and R01-CA138255 and via a Breast SPORE program (P50-CA58223). L. Makowski was supported by UNC University Cancer Research Fund, National Institute of Diabetes, Digestive and Kidney Disease (P30DK056350), National Institute of Alcohol Abuse and Alcoholism (AA017376), and National Institutes of Environmental Health Sciences and NCI (ES019472).

The costs of publication of this article were defrayed in part by the payment of page charges. This article must therefore be hereby marked *advertisement* in accordance with 18 U.S.C. Section 1734 solely to indicate this fact.

Received June 28, 2012; revised October 31, 2012; accepted November 20, 2012; published OnlineFirst December 12, 2012.

Downloaded from http://aacrjournals.org/clincancerres/article-pdf/19/3/571/2296963/571.pdf by guest on 24 August 2022

References

1. Garber K. Energy deregulation: licensing tumors to grow. Science 2006;312:1158–9.
2. Castello-Cros R, Bonnuccelli G, Molchansky A, Capozza F, Witkiewicz AK, Birbe RC, et al. Matrix remodeling stimulates stromal autophagy, "fueling" cancer cell mitochondrial metabolism and metastasis. Cell Cycle 2011;10:2021–34.
3. Gatenby RA, Gillies RJ. Why do cancers have high aerobic glycolysis? Nat Rev Cancer 2004;4:891–9.
4. Warburg O, Wind F, Negelein E. The Metabolism of tumors in the body. J Gen Physiol 1927;8:519–30.
5. Camp JT, Elloumi F, Roman-Perez E, Rein J, Stewart DA, Harrell JC, et al. Interactions with fibroblasts are distinct in Basal-like and luminal breast cancers. Mol Cancer Res 2011;9:3–13.
6. De Clerck YA, Weissman BE, Yu D, Parsons R, Bar-Eli M, Roy-Burman P, et al. Tumor progression and metastasis from genetic to microenvironmental determinants: a workshop of the tumor progression and metastasis NIH study section in honor of Dr. Martin L. Padarathsingh, May 31, 2006, Georgetown, Washington, DC. Cancer Biol Ther 2006; 5:1588–99.
7. Gatza ML, Kung HN, Blackwell KL, Dewhirst MW, Marks JR, Chi JT. Analysis of tumor environmental response and oncogenic pathway activation identifies distinct basal and luminal features in HER2-related breast tumor subtypes. Breast Cancer Res 2011; 13:R62.
8. Tlsty TD, Coussens LM. Tumor stroma and regulation of cancer development. Annu Rev Pathol 2006;1:119–50.
9. Martinez-Outschoorn UE, Balliet RM, Rivadeneira DB, Chiavarina B, Pavlides S, Wang C, et al. Oxidative stress in cancer associated fibroblasts drives tumor-stroma co-evolution: A new paradigm for understanding tumor metabolism, the field effect and genomic instability in cancer cells. Cell Cycle 2010;9:3256–76.
10. Martinez-Outschoorn UE, Pavlides S, Howell A, Pestell RG, Tanowitz HB, Sotgia F, et al. Stromal-epithelial metabolic coupling in cancer: integrating autophagy and metabolism in the tumor microenvironment. Int J Biochem Cell Biol 2011;43:1045–51.
11. Martinez-Outschoorn UE, Trimmer C, Lin Z, Whitaker-Menezes D, Chiavarina B, Zhou J, et al. Autophagy in cancer associated fibroblasts promotes tumor cell survival: Role of hypoxia, HIF1 induction and NFkappaB activation in the tumor stromal microenvironment. Cell Cycle 2010;9:3515–33.
12. Stewart DA, Yang Y, Makowski L, Troester MA. Basal-like breast cancer cells induce phenotypic and genomic changes in macrophages. Mol Cancer Res 2012;10:727–38.
13. Martinez-Outschoorn UE, Lin Z, Trimmer C, Flomenberg N, Wang C, Pavlides S, et al. Cancer cells metabolically "fertilize" the tumor microenvironment with hydrogen peroxide, driving the Warburg effect: implications for PET imaging of human tumors. Cell Cycle 2011;10: 2504–20.
14. Pavlides S, Whitaker-Menezes D, Castello-Cros R, Flomenberg N, Witkiewicz AK, Frank PG, et al. The reverse Warburg effect: aerobic glycolysis in cancer associated fibroblasts and the tumor stroma. Cell Cycle 2009;8:3984–4001.
15. Pavlides S, Tsirigos A, Vera I, Flomenberg N, Frank PG, Casimiro MC, et al. Transcriptional evidence for the "Reverse Warburg Effect" in human breast cancer tumor stroma and metastasis: similarities with oxidative stress, inflammation, Alzheimer's disease, and "Neuron-Glia Metabolic Coupling". Aging 2010;2: 185–99.
16. Pavlides S, Tsirigos A, Migneco G, Whitaker-Menezes D, Chiavarina B, Flomenberg N, et al. The autophagic tumor stroma model of cancer: role of oxidative stress and ketone production in fueling tumor cell metabolism. Cell Cycle 2010;9:3485–505.
17. Perou CM, Sorlie T, Eisen MB, van de Rijn M, Jeffrey SS, Rees CA, et al. Molecular portraits of human breast tumours. Nature 2000;406: 747–52.
18. Fan C, Prat A, Parker JS, Liu Y, Carey LA, Troester MA, et al. Building prognostic models for breast cancer patients using clinical variables and hundreds of gene expression signatures. BMC Med Genomics 2011;4:3.
19. Ross DT, Perou CM. A comparison of gene expression signatures from breast tumors and breast tissue derived cell lines. Dis Markers 2001;17:99–109.
20. Prat A, Parker JS, Karginova O, Fan C, Livasy C, Herschkowitz JI, et al. Phenotypic and molecular characterization of the claudin-low intrinsic subtype of breast cancer. Breast Cancer Res 2010;12:R68.
21. Santarpia L, Qi Y, Stemke-Hale K, Wang B, Young EJ, Booser DJ, et al. Mutation profiling identifies numerous rare drug targets and distinct mutation patterns in different clinical subtypes of breast cancers. Breast Cancer Res Treat 2012;134:333–43.
22. Rouzier R, Perou CM, Symmans WF, Ibrahim N, Cristofanilli M, Anderson K, et al. Breast cancer molecular subtypes respond differently to preoperative chemotherapy. Clin Cancer Res 2005;11: 5678–85.
23. Perou CM, Borresen-Dale AL. Systems biology and genomics of breast cancer. Cold Spring Harb Perspect Biol 2011;3. pii: a003293.
24. Radisky D, Hagios C, Bissell MJ. Tumors are unique organs defined by abnormal signaling and context. Semin Cancer Biol 2001;11:87–95.
25. Troester MA, Lee MH, Carter M, Fan C, Cowan DW, Perez ER, et al. Activation of host wound responses in breast cancer microenvironment. Clin Cancer Res 2009;15:7020–8.
26. Hu Z, Fan C, Oh DS, Marron JS, He X, Qaqish BF, et al. The molecular portraits of breast tumors are conserved across microarray platforms. BMC Genomics 2006;7:96.
27. Tusher VG, Tibshirani R, Chu G. Significance analysis of microarrays applied to the ionizing radiation response. Proc Natl Acad Sci U S A 2001;98:5116–21.
28. Page RD. Visualizing phylogenetic trees using TreeView. Curr Protoc Bioinformatics 2002;Chapter 6:Unit 6.2.
29. Creighton CJ, Nagaraja AK, Hanash SM, Matzuk MM, Gunaratne PH. A bioinformatics tool for linking gene expression profiling results with public databases of microRNA target predictions. RNA 2008; 14:2290–6.
30. Neve RM, Chin K, Fridlyand J, Yeh J, Baehner FL, Fevr T, et al. A collection of breast cancer cell lines for the study of functionally distinct cancer subtypes. Cancer Cell 2006;10:515–27.
31. Pelletier J, Bellot G, Gounon P, Lacas-Gervais S, Pouyssegur J, Mazure NM. Glycogen synthesis is induced in hypoxia by the hypoxia-inducible factor and promotes cancer cell survival. Front Oncol 2012;2:18.
32. Bonuccelli G, Whitaker-Menezes D, Castello-Cros R, Pavlides S, Pestell RG, Fatatis A, et al. The reverse Warburg effect: glycolysis inhibitors prevent the tumor promoting effects of caveolin-1 deficient cancer associated fibroblasts. Cell Cycle 2010;9:1960–71.
33. Pavlides S, Vera I, Gandara R, Sneddon S, Pestell RG, Mercier I, et al. Warburg meets autophagy: cancer-associated fibroblasts accelerate tumor growth and metastasis via oxidative stress, mitophagy, and aerobic glycolysis. Antioxid Redox Signal 2012;16:1264–84.
34. Zhao FQ, Keating AF. Functional properties and genomics of glucose transporters. Curr Genomics 2007;8:113–28.
35. Kang SS, Chun YK, Hur MH, Lee HK, Kim YJ, Hong SR, et al. Clinical significance of glucose transporter 1 (GLUT1) expression in human breast carcinoma. Jap J Cancer Res 2002;93:1123–8.
36. Young CD, Lewis AS, Rudolph MC, Ruehle MD, Jackman MR, Yun UJ, et al. Modulation of glucose transporter 1 (GLUT1) expression levels alters mouse mammary tumor cell growth *in vitro* and *in vivo*. PloS One 2011;6:e23205.
37. Perdomo G, Martinez-Brocca MA, Bhatt BA, Brown NF, O'Doherty RM, Garcia-Ocana A. Hepatocyte growth factor is a novel stimulator of glucose uptake and metabolism in skeletal muscle cells. J Biol Chem 2008;283:13700–6.
38. Gillies RJ, Gatenby RA. Hypoxia and adaptive landscapes in the evolution of carcinogenesis. Cancer Metastasis Rev 2007;26:311–7.
39. Robey IF, Stephen RM, Brown KS, Baggett BK, Gatenby RA, Gillies RJ. Regulation of the Warburg effect in early-passage breast cancer cells. Neoplasia 2008;10:745–56.
40. Wang H, Tso VK, Slupsky CM, Fedorak RN. Metabolomics and detection of colorectal cancer in humans: a systematic review. Future Oncol 2010;6:1395–406.

Downloaded from http://aacrjournals.org/clincancerres/article-pdf/19/3/571/2296963/571.pdf by guest on 24 August 2022

41. Sitter B, Lundgren S, Bathen TF, Halgunset J, Fjosne HE, Gribbestad IS. Comparison of HR MAS MR spectroscopic profiles of breast cancer tissue with clinical parameters. NMR Biomed 2006;19:30–40.
42. Oakman C, Tenori L, Biganzoli L, Santarpia L, Cappadona S, Luchinat C, et al. Uncovering the metabolomic fingerprint of breast cancer. Int J Biochem Cell Biol 2011;43:1010–20.
43. Lisanti MP, Martinez-Outschoorn UE, Chiavarina B, Pavlides S, Whitaker-Menezes D, Tsirigos A, et al. Understanding the "lethal" drivers of tumor-stroma co-evolution: emerging role(s) for hypoxia, oxidative stress and autophagy/mitophagy in the tumor micro-environment. Cancer Biol Ther 2010;10:537–42.
44. Brockmoller SF, Bucher E, Muller BM, Budczies J, Hilvo M, Griffin JL, et al. Integration of metabolomics and expression of glycerol-3-phosphate acyltransferase (GPAM) in breast cancer-link to patient survival, hormone receptor status, and metabolic profiling. J Proteome Res 2012;11:850–60.
45. Bissell MJ, Hines WC. Why don't we get more cancer? A proposed role of the microenvironment in restraining cancer progression. Nat Med 2011;17:320–9.
46. Bissell MJ, Radisky D. Putting tumours in context. Nat Rev Cancer 2001;1:46–54.
47. Sieweke MH, Thompson NL, Sporn MB, Bissell MJ. Mediation of wound-related Rous sarcoma virus tumorigenesis by TGF-beta. Science 1990;248:1656–60.
48. Borgan E, Sitter B, Lingjaerde OC, Johnsen H, Lundgren S, Bathen TF, et al. Merging transcriptomics and metabolomics–advances in breast cancer profiling. BMC Cancer 2010;10:628.
49. Denkert C, Bucher E, Hilvo M, Salek R, Oresic M, Griffin J, et al. Metabolomics of human breast cancer: new approaches for tumor typing and biomarker discovery. Genome Med 2012;4:37.
50. Giskeodegard GF, Lundgren S, Sitter B, Fjosne HE, Postma G, Buydens LM, et al. Lactate and glycine-potential MR biomarkers of prognosis in estrogen receptor-positive breast cancers. NMR Biomed 2012;25:1271–9.
51. Ferrara CT, Wang P, Neto EC, Stevens RD, Bain JR, Wenner BR, et al. Genetic networks of liver metabolism revealed by integration of metabolic and transcriptional profiling. PLoS Genetics 2008;4:e1000034.
52. Capparelli C, Guido C, Whitaker-Menezes D, Bonuccelli G, Balliet R, Pestell TG, et al. Autophagy and senescence in cancer-associated fibroblasts metabolically supports tumor growth and metastasis via glycolysis and ketone production. Cell Cycle 2012;11:2285–302.
53. Bhargava M, Joseph A, Knesel J, Halaban R, Li Y, Pang S, et al. Scatter factor and hepatocyte growth factor: activities, properties, and mechanism. Cell Growth Differ 1992;3:11–20.
54. Taher TE, Derksen PW, de Boer OJ, Spaargaren M, Teeling P, van der Wal AC, et al. Hepatocyte growth factor triggers signaling cascades mediating vascular smooth muscle cell migration. Biochem Biophys Res Commun 2002;298:80–6.
55. Birchmeier C, Birchmeier W, Gherardi E, Vande Woude GF. Met, metastasis, motility and more. Nat Rev Mol Cell Biol 2003;4:915–25.
56. Trusolino L, Bertotti A, Comoglio PM. MET signalling: principles and functions in development, organ regeneration and cancer. Nat Rev Mol Cell Biol 2010;11:834–48.
57. Naldini L, Vigna E, Narsimhan RP, Gaudino G, Zarnegar R, Michalopoulos GK, et al. Hepatocyte growth factor (HGF) stimulates the tyrosine kinase activity of the receptor encoded by the proto-oncogene c-MET. Oncogene 1991;6:501–4.
58. Weidner KM, Arakaki N, Hartmann G, Vandekerckhove J, Weingart S, Rieder H, et al. Evidence for the identity of human scatter factor and human hepatocyte growth factor. Proc Natl Acad Sci U S A 1991;88:7001–5.
59. Previdi S, Maroni P, Matteucci E, Broggini M, Bendinelli P, Desiderio MA. Interaction between human-breast cancer metastasis and bone microenvironment through activated hepatocyte growth factor/Met and beta-catenin/Wnt pathways. Eur J Cancer 2010;46:1679–91.
60. Gos M, Miloszewska J, Przybyszewska M. [Epithelial-mesenchymal transition in cancer progression]. Postepy Biochemii 2009;55:121–8.
61. Lam MM, Swanson PE, Upton MP, Yeh MM. Ovarian-type stroma in hepatobiliary cystadenomas and pancreatic mucinous cystic neoplasms: an immunohistochemical study. Am J Clin Pathol 2008;129:211–8.
62. Felix AS, Edwards RP, Stone RA, Chivukula M, Parwani AV, Bowser R, et al. Associations between hepatocyte growth factor, c-Met, and basic fibroblast growth factor and survival in endometrial cancer patients. Br J Cancer 2012;106:2004–9.
63. Straussman R, Morikawa T, Shee K, Barzily-Rokni M, Qian ZR, Du J, et al. Tumour micro-environment elicits innate resistance to RAF inhibitors through HGF secretion. Nature 2012;487:500–4.
64. Cheng N, Chytil A, Shyr Y, Joly A, Moses HL. Enhanced hepatocyte growth factor signaling by type II transforming growth factor-beta receptor knockout fibroblasts promotes mammary tumorigenesis. Cancer Res 2007;67:4869–77.
65. Hwang CI, Choi J, Zhou Z, Flesken-Nikitin A, Tarakhovsky A, Nikitin AY. MET-dependent cancer invasion may be preprogrammed by early alterations of p53-regulated feedforward loop and triggered by stromal cell-derived HGF. Cell Cycle 2011;10:3834–40.
66. Shojaei F, Simmons BH, Lee JH, Lappin PB, Christensen JG. HGF/c-Met pathway is one of the mediators of sunitinib-induced tumor cell type-dependent metastasis. Cancer Lett 2012;320:48–55.
67. Gastaldi S, Comoglio PM, Trusolino L. The Met oncogene and basal-like breast cancer: another culprit to watch out for? Breast Cancer Res 2010;12:208.
68. Mueller KL, Madden JM, Zoratti GL, Kuperwasser C, List K, Boerner JL. Fibroblast-secreted hepatocyte growth factor mediates epidermal growth factor receptor tyrosine kinase inhibitor resistance in triple-negative breast cancers through paracrine activation of Met. Breast Cancer Res 2012;14:R104.
69. Yasui T, Ohuchida K, Zhao M, Onimaru M, Egami T, Fujita H, et al. Tumor-stroma interactions reduce the efficacy of adenoviral therapy through the HGF-MET pathway. Cancer Sci 2011;102:484–91.
70. Potenta S, Zeisberg E, Kalluri R. The role of endothelial-to-mesenchymal transition in cancer progression. Br J Cancer 2008;99:1375–9.
71. Whitaker-Menezes D, Martinez-Outschoorn UE, Lin Z, Ertel A, Flomenberg N, Witkiewicz AK, et al. Evidence for a stromal-epithelial "lactate shuttle" in human tumors: MCT4 is a marker of oxidative stress in cancer-associated fibroblasts. Cell Cycle 2011;10:1772–83.

Downloaded from http://aacrjournals.org/clincancerres/article-pdf/19/3/571/2296963/571.pdf by guest on 24 August 2022